

Supplementary Information

Sources and light absorption of water-soluble organic carbon aerosols in the outflow from northern China

Elena N. Kirillova, August Andersson, Jihyun Han, Meehye Lee and Örjan Gustafsson

Text

Back trajectories analysis

Five-day back trajectories (BTs) at heights 850m, 500m and 100m (a.g.l.) were generated for every 6 hours during the GoPoEx campaign using NOAA HYSPLIT software v4 (<http://www.arl.noaa.gov/ready/hysplit4.html>). The BTs representing each sample (Fig. S1-3) were grouped into five groups.

The Beijing group covers air masses passing over the Beijing region at low altitudes. This group include the BTs of samples 1, partially 2, 5-7 and 16 collected on 8-9, 11-12 and 16 March 2011. 5-day BTs of this group originated from Mongolia, Russian Siberia to the south of Lake Baikal or Nei Mongol province of China and then passed Nei Mongol, Heibei, Tianjing, Shandong and partially Liaoning provinces of China, including Beijing area. BTs dipped down to the surface level and subsequently rose to the levels 850m, 500m and 100m 1-2 days before arriving to the Gosan station (Fig. S1). Sample 16 collected in the afternoon of 16 March represented air masses that had travelled slightly longer distance and is characterized by higher wind speeds upon arrival at KCOG (Fig. S2).

The Liaoning group starts on 9 March from sample 2, representing the transition from Beijing group, and continues until 10 March including samples 3, 4 and also observed on the 21-22 March during the collection of sample 26. It had very similar BT origin and height variation as Beijing group but the path of BTs did not cross Beijing area but rather passed Liaoning province (Fig. S1, S3).

The Yellow Sea group includes air masses circulating at high altitude over Jeju Island region. The group includes the BTs of samples 8, 9, 10 and 11 and partially 12 collected 12-15 March 2011 and samples 20, 21, 22 collected 18-20 March 2011. Initially, BT path for these samples was similar to Beijing and Liaoning groups (Fig. S1-3). However, already 2-4 days back in time the air masses reached the Yellow Sea coast and rise to the 850-900m, 500-600m or 100-200m level at which they circulated until they reached Jeju Island. Sample 12 represents the transition of air masses from the circulation above the Yellow sea at heights for more than 5 days to the outflow from Southern Siberia at the Chinese border through Nei Mongol, Jilin and Liaoning provinces of China.

The Mongol group contains air masses that originate over Mongolia and the Nei Mongol province in China. This relatively longer transport is characterized by higher wind speeds. The Mongol group combines the BTs of samples 13, 14, 15, 17 and 18 collected 15-18 March 2011 (Fig. S2). The air masses during this period travelled the longest distance compared to other trajectory groups.

The Korea group includes air masses passing over the Korean peninsula. It includes BTs of samples 23, 24 and 25 collected during 20-21 March 2011 (Fig. S3). 5-day BTs started from circulation at height above the Yellow Sea coast and dipped down to the ground level at the Korean peninsula about one day before arrival to KCOG above the Yellow Sea at height of 600m.

Selected samples for carbon isotope analysis

Initially ten sampling periods during the GoPoEx were selected for carbon isotope analysis. Two criteria were used to guide this selection: different source areas in China judging from BT analysis and carbonaceous material loadings on the filters had to be enough for the isotope analysis of the main carbon fractions. Samples number 1, 5, 6, 7, 11, 12, 13, 16, 20 and 26 were chosen for the analysis. The samples of Beijing group (1, 5, 6, and 7) had the highest loadings. Samples 5, 6 and 7 represented the concentration peak in all carbonaceous fractions (TC, WSOC, EC) (Fig. 2, Fig. S4). Sample 11 was from the Yellow Sea group. Sample 12 was characterized by the transition of the air masses from long circulation over the Yellow Sea to the long-distance pathway through Russia, Mongolia and Nei Mongol province of China (Mongol group). Sample 13 represented Mongol group and it was affected by dust. Sample 16 had relatively high loadings of TC and WSOC, and BTs for the period of its sampling were passing Beijing area. Sample 20 represented Yellow Sea group but BTs at 850m represented the most southern source areas in China (Shanxi, Henan, Anhui, Zhejiang provinces) during the sampling campaign so that it can be influenced by different pollution sources than other samples in this group. Sample 26 represented Liaoning group and was also influenced by Asian dust episode and minor pollution plume.

Additionally, ten more samples number 3, 4, 9, 10, 14, 15, 18, 21, 23 and 25 from each back trajectory group were used for TOC and WSOC stable carbon isotope analysis

Direct absorptive radiative forcing of WSOC relative to elemental carbon (EC)

The amount of solar energy absorbed by WSOC relative to elemental carbon (EC) is estimated using a simplistic model. Elemental carbon (EC) is a common operationally-defined estimate of black carbon (BC) – the most efficient light absorbing aerosol species. In this model, the solar emission (I_0) is approximate though the wavelength-dependent clear sky Air

Mass 1 Global Horizontal (AM1GH) solar irradiance model (Fig. S7), which includes light absorption by, e.g., ozone and water (Levinson et al., 2010).

The wavelength-dependent fraction sunlight absorbed by aerosol species X, where X is either BC or WSOC, is given by combining the Lambert-Beer law with the wavelength-dependence of the *MAC* (given by Equations (1) and (2) in the main text):

$$\frac{I_0 - I}{I_0}(\lambda, X) = 1 - e^{-\left(MAC_{\lambda_0, X} \left(\frac{\lambda_0}{\lambda} \right)^{AAE_X} \cdot C_X \cdot h_{ABL} \right)} \quad (S1)$$

Where $MAC_{\lambda_0, X}$ is the mass absorption cross section at a given reference wavelength ($\lambda_{0, WSOC} = 365\text{nm}$, $\lambda_{0, EC} = 520\text{nm}$), AAE_X is the absorption Ångström exponent for X, h_{ABL} is the height of the atmospheric boundary layer (ABL) and C_X is the concentration of X. Combining Equations (S1) and (S2) we can compute the fraction solar energy (f) absorbed by WSOC relative to EC as:

$$f = \frac{\int I_0(\lambda) \cdot \frac{I_0 - I}{I_0}(\lambda, WSOC) d\lambda}{\int I_0(\lambda) \cdot \frac{I_0 - I}{I_0}(\lambda, BC) d\lambda} \quad (S2)$$

The fraction f was computed using numerical integration using measured sample (filter) specific values for the concentrations of WSOC and EC, and the optical properties of WSOC (MAC_{365} and AAE). The h_{ABL} is set to 1000m, but has little influence on the computed ratio in the range of 200 – 3000m. The *MAC* for EC is a matter of considerable debate. The *MAC*-values for EC depend on both the degree and structure of the internal/external mixing of different aerosol constituents, and also on the emission source (Cheng et al., 2011; Bond et al., 2006). Generally the *MAC* of EC is increased due to internal mixing effects, but it is not clear how much this mixing would increase the *MAC* of other absorbing aerosol components, i.e., brown carbon or dust. Here it is for simplicity assumed that any enhancements of *MAC* due to mixing effects are the same for EC and WSOC.

For China, the *MAC*-values for EC span a range of values. Yang et al. reported $MAC_{550,EC} = 9.5 \text{ m}^2/\text{g}$ values near Beijing (Yang et al., 2009), which are similar to the values by Cheng et al. (2011), $MAC_{632,EC} = 8.45 \pm 1.71 \text{ m}^2/\text{g}$ (winter) and $9.41 \pm 1.92 \text{ m}^2/\text{g}$ (summer), and Lan et al. (2013) reported values of $MAC_{532,EC} = 6.5 \pm 0.5 \text{ m}^2/\text{g}$ at an urban site in south China. Here we used the value suggested by Chung et al. (2012), $MAC_{520,EC} = 5.6 \text{ m}^2/\text{g}$, derived for the sampling site used during the GoPoEx (KCOG). However, a range of values ($MAC_{520,EC} = 4 - 12 \text{ m}^2/\text{g}$) was also examined, to investigate the influence of this parameter (Fig. S8). The AAE for EC was set to 1.

This simplistic estimate, which is similar to the approach of Kirchstetter and Thatcher (2012), is based on several assumptions: AAE for WSOC measured at 330 – 400nm represents the whole spectral range (no difference in calculated relative forcing was detected when using the raw absorption data), the light-absorptive properties of the solvent extracts are representative of the ambient aerosol phase, the assumptions regarding MAC_{550} and AAE for EC are reasonable, the measurements at ground level represents the whole ABL, the solar light may be approximated using a black body model, no effects of scattering (aerosols or cloud droplets) or size distributions of aerosols are included. However, the rationale for this calculation is not to provide a precise estimate of the radiative forcing of WSOC per se, but to provide a first field-observation-based relative estimate of WSOC vs EC in the outflow from N China, emphasizing the need to consider WSOC sunlight absorption in climate models.

Error analysis and Monte Carlo based uncertainty estimates

The overall precision in the TOC and WSOC concentrations and isotopic signatures was estimated considering the precision of concentration estimation (estimates from triplicate analysis), mass contributions from field blanks (estimates from several blanks), as well as precision of isotope characterization (instrument precision) and the isotope signature of the field blanks. To obtain the overall precision, these factors need to be combined using an error

propagation scheme. Here, this was implemented using a Monte Carlo strategy. In this procedure, the uncertainty for each parameter (e.g., field blank concentration) was represented by a normal distribution with zero mean and a standard deviation equal to the measured uncertainty (Kirillova et al., 2013).

Independent random samplings from the distributions representing the data were performed using an in-house written Matlab script. For each point, 10000 iterations of the random sampling scheme were conducted, allowing all major combinations to be sampled. The overall precision of a given parameter is estimated as the standard deviation for all 10000 computed solutions.

To account for the uncertainty in the fractional contributions of radiocarbon-extinct fossil fuel sources vs contemporary biomass/biogenic sources the endmember variability was incorporated in the assessment (Andersson, 2011). Fraction fossil (f_{fossil}) was determined using the isotopic mass balance equation:

$$\Delta^{14}\text{C}_{\text{sample}} = \Delta^{14}\text{C}_{\text{fossil}} \times f_{\text{fossil}} + \Delta^{14}\text{C}_{\text{biomass}} \times (1 - f_{\text{fossil}}) \quad (\text{S3})$$

where $\Delta^{14}\text{C}_{\text{sample}}$ is the measured radiocarbon content of a WSOC sample and $\Delta^{14}\text{C}_{\text{fossil}}$ is -1000‰. The $\Delta^{14}\text{C}_{\text{biomass}}$ endmember is between +50‰ and +225‰. The first value corresponds to the $\Delta^{14}\text{C}$ of contemporary CO_2 (Levin et al., 2010; Graven et al., 2012), and thus freshly produced biomass. The second value is for the $\Delta^{14}\text{C}$ of wood logged in the 1990s-2000s (Zencak et al., 2007; Klinedinst and Currie, 1999). For East Asia biomass burning the end-member value of +112‰ have been estimated based on relative contribution from contemporary (meaning one-year plants) biofuel and wood fuel (Chen et al., 2013). In the absence of such detailed information and since the relative contributions to WSOC from biogenic secondary organic aerosols (SOA) and from biomass burning primary organic aerosols (POA) and SOA are not known *a priori*, they were here assumed to be of equal

importance. Hence, the biogenic/biomass $\Delta^{14}\text{C}$ endmember for WSOC was set to +81‰, which is the mean value of +50‰ and +112‰.

References:

Andersson, A.: A systematic examination of a random sampling strategy for source apportionment calculations, *Sci. Tot. Environ.*, 412-413, 232-238, 2011.

Bond, T.C., Habib, G., Bergstrom, R.W.: Limitations in the enhancement of visible light absorption due to mixing state, *J. Geophys. Res.*, 111, DOI: 10.1029/2006JD007315, 2006.

Chen, B., Andersson, A., Lee M., Kirillova, E., Xiao, Q., Kruså, M., Shi, M., Hu, K., Lu, Z., Street, D.G., Du, K., and Gustafsson, Ö. Source forensics of black carbon aerosols from China, *Environ. Sci. Technol.*, 47, 9102-9108, 2013.

Cheng, Y., He, K.-B., Zheng, M., Duan, F.-K., Du, Z.-Y., Ma, Y.-L., Tan, J.-H., Yang, F.-M., Liu, J.-M., Zhang, X.-L., Weber, R.J., Bergin, M. H., and Russell, A. G: Mass absorption efficiency of elemental carbon and water-soluble organic carbon in Beijing, China, *Atmos. Chem. Phys.*, 11, 11497-11510, 2011.

Chung, C.E., Kim, S.W., Lee, M., Yoon, S.C., Lee, S.: Carbonaceous aerosol AAE inferred from in-situ aerosol measurements at the Gosan ABC super site, and the implications for brown carbon aerosol, *Atmos. Chem. Phys.*, 12, 6173-6184, 2012.

Graven, H.D., Guilderson, T.P., Keeling, R.F.: Observations of radiocarbon in CO₂ at seven global sampling sites in the Scripps flask network: Analysis of spatial gradients and seasonal cycles, *J. Geophys. Res.*, 117, D02303, 2012.

Kirchstetter, T.W., Thatcher, T.L.: Contribution of organic carbon to wood smoke particulate matter absorption of solar radiation, *Atmos. Chem. Phys.*, 12, 6067-6072, 2012.

Kirillova, E.N., Andersson A., Sheesley R. J., Krusa M., Praveen P. S., Budhavant K., Safai P. D., Rao P. S. P. and Gustafsson O.: ^{13}C - and ^{14}C -based study of sources and atmospheric processing of water-soluble organic carbon (WSOC) in South Asian aerosols, *J. Geophys. Res.*, 118, 614–626, 2013.

Klinedinst, D.B. and Currie, L.A.: Direct quantification of $\text{PM}_{2.5}$ fossil and biomass carbon within the Northern Front Range Air Quality Study's domain, *Environ. Sci. Technol.*, 33, 4146–4154, 1999.

Lan, Z.-J., Huang, X.-F., Yu, K.-Y., Sun, T.-L., Zeng, L.-W., Hu, M.: Light absorption of black carbon aerosol and its enhancement by mixing state in an urban atmosphere in South China, *Atmos. Environ.*, 69, 118-123, 2013.

Levin, I., Naegler, T., Kromer, B., Diehl, M., Francey, R.J., Gomez-Pelaez, A.J., Steele, L.P., Wagenbach, D., Weller, R., and Worthy, D.E.: Observations and modelling of the global distribution and long-term trend of atmospheric $^{14}\text{CO}_2$, *Tellus B*, 62, 26–46, 2010.

Levinson, R., Akbari, H., Berdahl, P.: Measuring solar reflectance – Part I: defining a metric that accurately predicts solar heat gain, *Solar Energy*, 84, 1717-1744, 2010.

Yang, M., Howell, S.G., Zhuang, J., Huebert, B.J.: Attribution of aerosol light absorption to black carbon, brown carbon and dust in China – interpretations of atmospheric measurements during EAST-AIRE, *Atmos. Chem. Phys.*, 9, 2035-2050, 2009.

Zencak, Z., Elmquist, M., Gustafsson, O.: Quantification and radiocarbon source apportionment of black carbon in atmospheric aerosols using the CTO-375 method, *Atmos. Environ.*, 41, 7895–7906, 2007.

Table S1. GoPoEx TSP and PM_{2.5} aerosol filter samples with duration and attribution to back trajectory groups.

Figure S1. NOAA HYSPLIT Back-Trajectories at heights 850m, 500m and 100m for samples 1-9.

Figure S2. NOAA HYSPLIT Back-Trajectories at heights 850m, 500m and 100m for samples 10-18.

Figure S3. NOAA HYSPLIT Back-Trajectories at heights 850m, 500m and 100m for samples 20-26.

Figure S4. Concentrations of total carbon (TC) (panel A); fraction fossil of total organic carbon (TOC) (panel B); stable carbon ratio in TOC (panel C) and water-soluble organic carbon (WSOC) (panel D); Absorption Ångström Exponents (AAE) for water-soluble organic carbon (WSOC) during GoPoEx campaign (panel E).

Figure S5. Wavelength dependent absorption spectra with the linear Ångström absorption coefficient (AAE) fitting for 13 TSP and PM_{2.5} samples extracted.

Figure S6. Relationship of the light attenuation coefficient (ATN) at 365 nm of the solution and the concentration of WSOC in the solution for 13 PM_{2.5} and TSP extracts.

Figure S7. Plot showing the AM1GH model for solar irradiance, used for calculations of the relative radiative forcing model in Equations S1-2 (Levinson et al., 2010).

Figure S8. Dependency of the relative radiative forcing WSOC/EC, calculated using Equation (S3), on the value of MAC_{520,EC}. Two samples are depicted: sample 6 from the Beijing pollution plume and sample 10 from the Yellow Sea back trajectory cluster, for two size fractions (PM_{2.5} and TSP). The vertical line emphasize MAC_{520,EC} = 5.6 m²/g (Chung et al., 2012) used in this paper.

Figure S9. Normalized wavelength-dependence of the absorptive radiative forcing of water-soluble brown carbon (WSOC, red) relative to black carbon (BC, black) for observation of their light absorption in samples of the outflow originating in N China and intercepted during GoPoEx computed using the model outlined in SI Text.

Figure S10. Concentrations of inorganic ions during GoPoEx campaign. Concentration of sodium (panel A). Concentrations of estimated non-sea salt sulfate, potassium and calcium and their relative fraction (as area plot for TSP and line plot for PM_{2.5}) of total measured concentration (panels B-D).

Table S1. GoPoEx TSP and PM2.5 aerosol filter samples with duration and attribution to back trajectory groups.

| Sample number | Sample number for isotope analysis | Group according to BTs analysis | Start Korean time | Stop Korean time | Start UTC | Stop UTC |
|---------------|------------------------------------|---------------------------------|-------------------|------------------|-----------------|-----------------|
| 1 | 1 | Beijing | 3/8/2011 12:25 | 3/9/2011 6:04 | 3/8/2011 3:25 | 3/8/2011 21:04 |
| 2 | | Beij./Liaon. | 3/9/2011 7:17 | 3/9/2011 20:52 | 3/8/2011 22:17 | 3/9/2011 11:52 |
| 3 | | Liaoning | 3/9/2011 22:31 | 3/10/2011 12:58 | 3/9/2011 13:31 | 3/10/2011 3:58 |
| 4 | | Liaoning | 3/10/2011 13:42 | 3/10/2011 21:10 | 3/10/2011 4:42 | 3/10/2011 12:10 |
| 5 | 2 | Beijing | 3/10/2011 21:47 | 3/11/2011 9:02 | 3/10/2011 12:47 | 3/11/2011 0:02 |
| 6 | 3 | Beijing | 3/11/2011 9:27 | 3/11/2011 18:33 | 3/11/2011 0:27 | 3/11/2011 9:33 |
| 7 | 4 | Beijing | 3/11/2011 19:08 | 3/12/2011 6:02 | 3/11/2011 10:08 | 3/11/2011 21:02 |
| 8 | | Yellow Sea | 3/12/2011 6:29 | 3/12/2011 21:15 | 3/11/2011 21:29 | 3/12/2011 12:15 |
| 9 | | Yellow Sea | 3/12/2011 21:43 | 3/13/2011 9:14 | 3/12/2011 12:43 | 3/13/2011 0:14 |
| 10 | | Yellow Sea | 3/13/2011 9:41 | 3/14/2011 6:06 | 3/13/2011 0:41 | 3/13/2011 21:06 |
| 11 | 5 | Yellow Sea | 3/14/2011 6:43 | 3/14/2011 20:14 | 3/13/2011 21:43 | 3/14/2011 11:14 |
| 12 | 6 | Y.Sea/Mong. | 3/14/2011 20:33 | 3/15/2011 4:37 | 3/14/2011 11:33 | 3/14/2011 19:37 |
| 13 | 7 | Mongol | 3/15/2011 5:01 | 3/15/2011 13:25 | 3/14/2011 20:01 | 3/15/2011 4:25 |
| 14 | | Mongol | 3/15/2011 13:53 | 3/16/2011 0:31 | 3/15/2011 4:53 | 3/15/2011 15:31 |
| 15 | | Mongol | 3/16/2011 0:43 | 3/16/2011 13:28 | 3/15/2011 15:43 | 3/16/2011 4:28 |
| 16 | 8 | Beijing | 3/16/2011 13:47 | 3/16/2011 22:41 | 3/16/2011 4:47 | 3/16/2011 13:41 |
| 17 | | Mongol | 3/16/2011 22:50 | 3/17/2011 22:55 | 3/16/2011 13:50 | 3/17/2011 13:55 |
| 18 | | Mongol | 3/17/2011 23:03 | 3/18/2011 10:09 | 3/17/2011 14:03 | 3/18/2011 1:09 |
| 19 | | | 3/18/2011 10:31 | Pump failure | 3/18/2011 1:31 | Pump failure |
| 20 | 9 | Yellow Sea | 3/19/2011 5:16 | 3/19/2011 18:00 | 3/18/2011 20:16 | 3/19/2011 9:00 |
| 21 | | Yellow Sea | 3/19/2011 18:56 | 3/20/2011 13:32 | 3/19/2011 9:56 | 3/20/2011 4:32 |
| 22 | | Yellow Sea | 3/20/2011 14:00 | 3/20/2011 21:50 | 3/20/2011 5:00 | 3/20/2011 12:50 |
| 23 | | Korea | 3/20/2011 21:58 | 3/21/2011 1:46 | 3/20/2011 12:58 | 3/20/2011 16:46 |
| 24 | | Korea | 3/21/2011 1:57 | 3/21/2011 12:49 | 3/20/2011 16:57 | 3/21/2011 3:49 |
| 25 | | Korea | 3/21/2011 12:59 | 3/21/2011 20:24 | 3/21/2011 3:59 | 3/21/2011 11:24 |
| 26 | 10 | Liaoning | 3/21/2011 20:32 | 3/22/2011 5:29 | 3/21/2011 11:32 | 3/21/2011 20:29 |

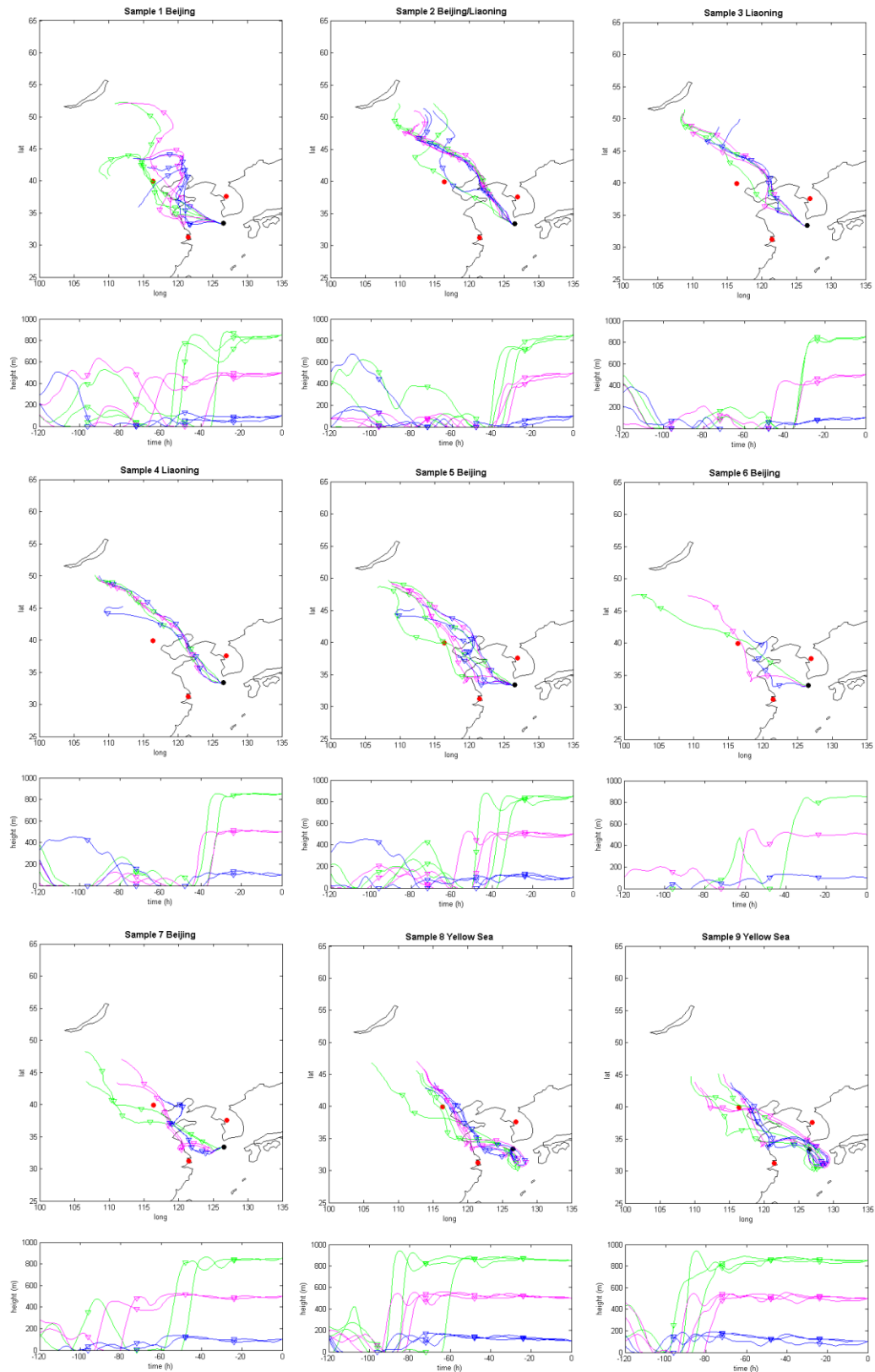


Figure S1 NOAA HYSPLIT Back-Trajectories at heights 850m, 500m and 100m for samples 1-9.

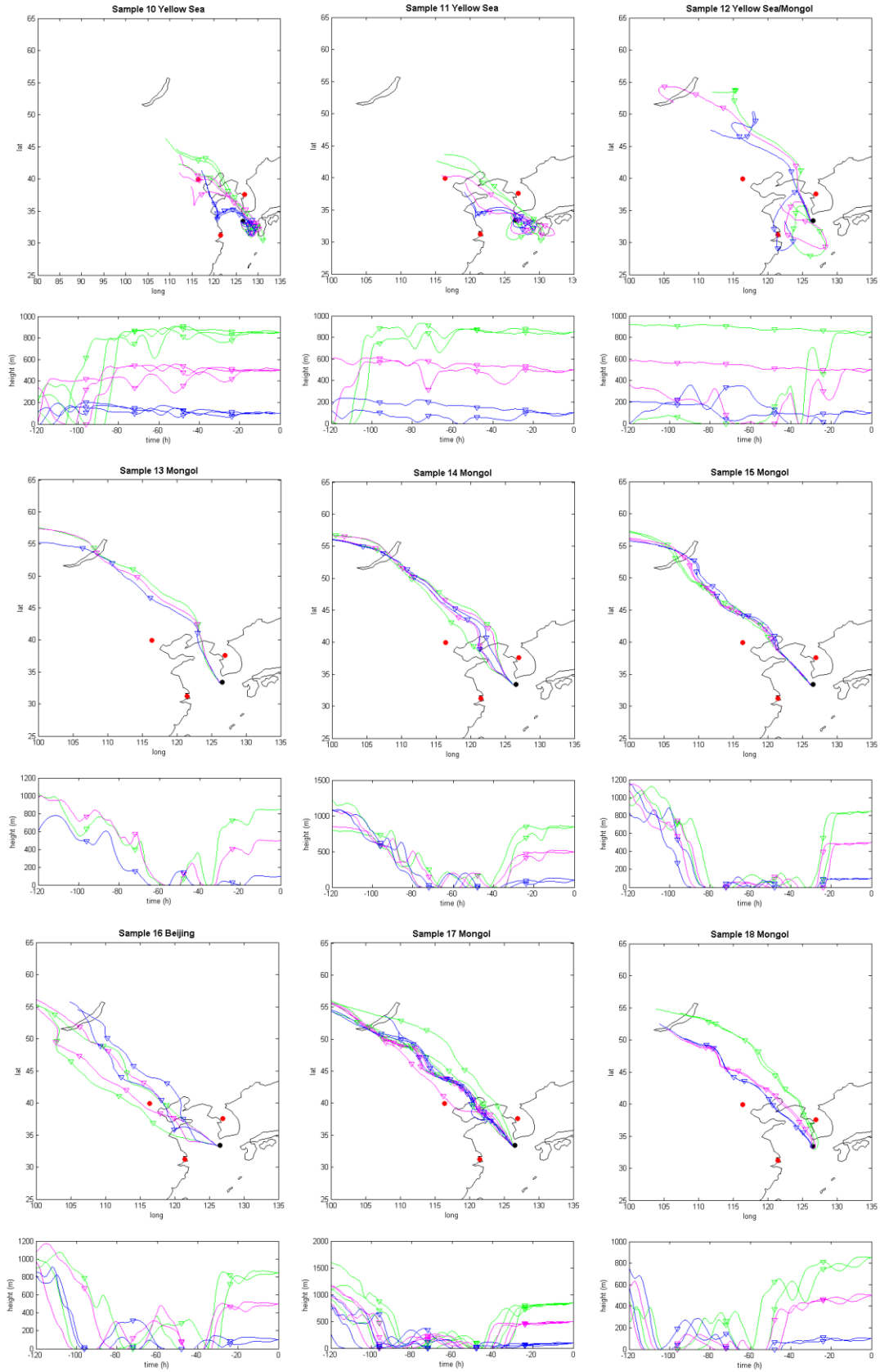


Figure S2 NOAA HYSPLIT Back-Trajectories at heights 850m, 500m and 100m for samples 10-18.

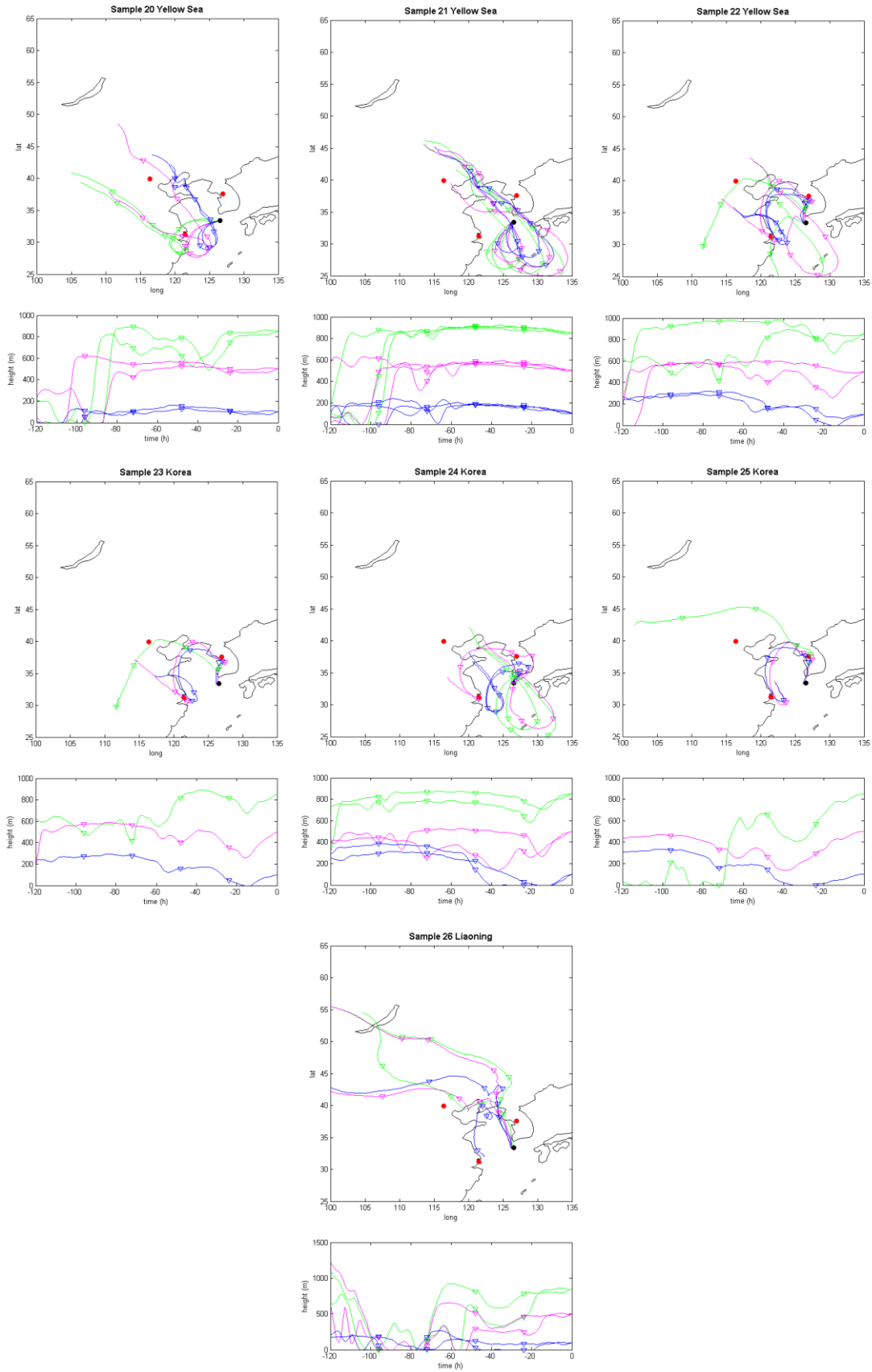


Figure S3 NOAA HYSPLIT Back-Trajectories at heights 850m, 500m and 100m for samples 20-26.

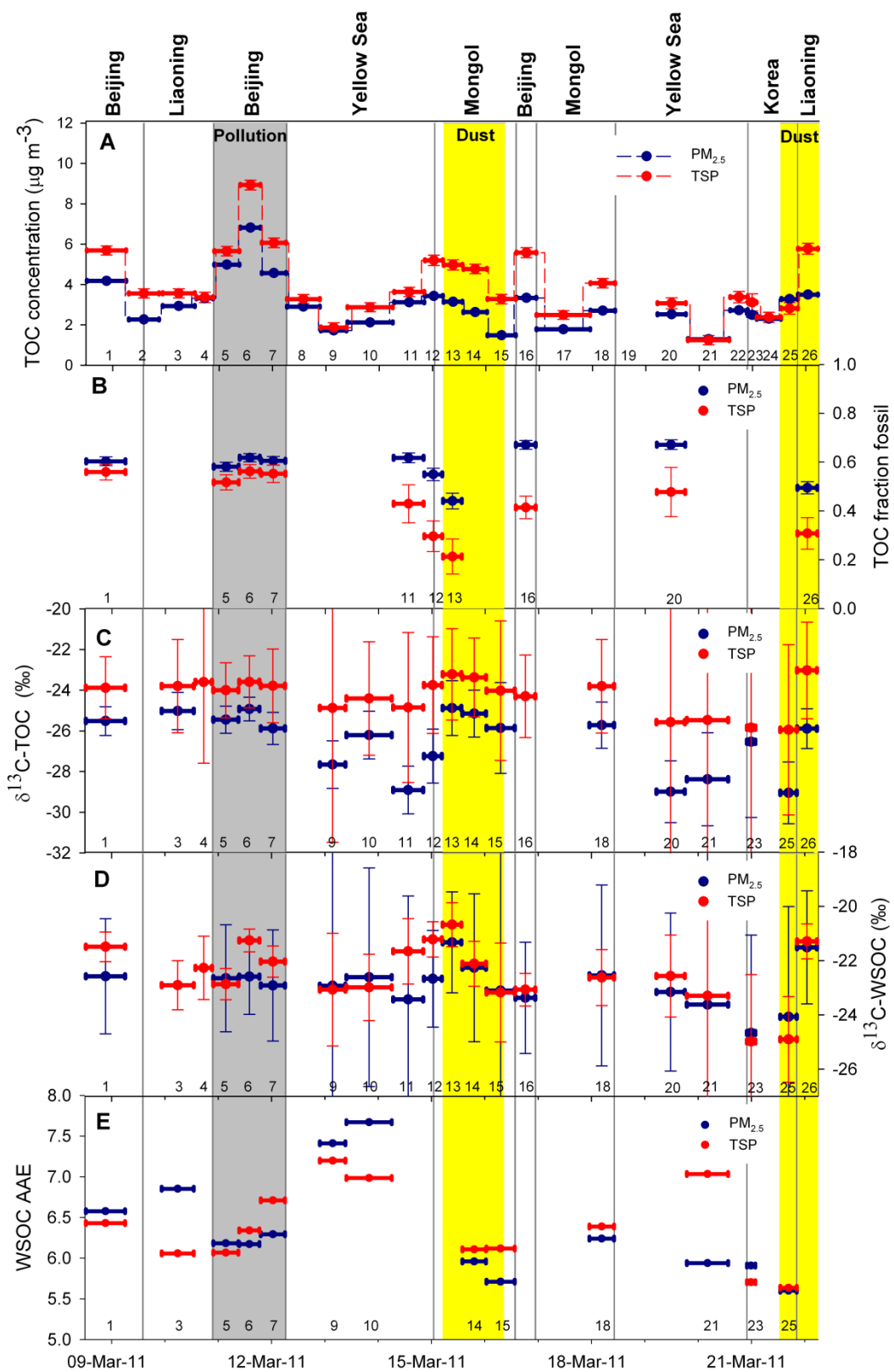


Figure S4. Concentrations of total carbon (TC) (panel A); fraction fossil of total organic carbon (TOC) (panel B); stable carbon ratio in TOC (panel C) and water-soluble organic carbon (WSOC) (panel D); Absorption Ångström Exponents (AAE) for water-soluble organic carbon (WSOC) during GoPoEx campaign (panel E).

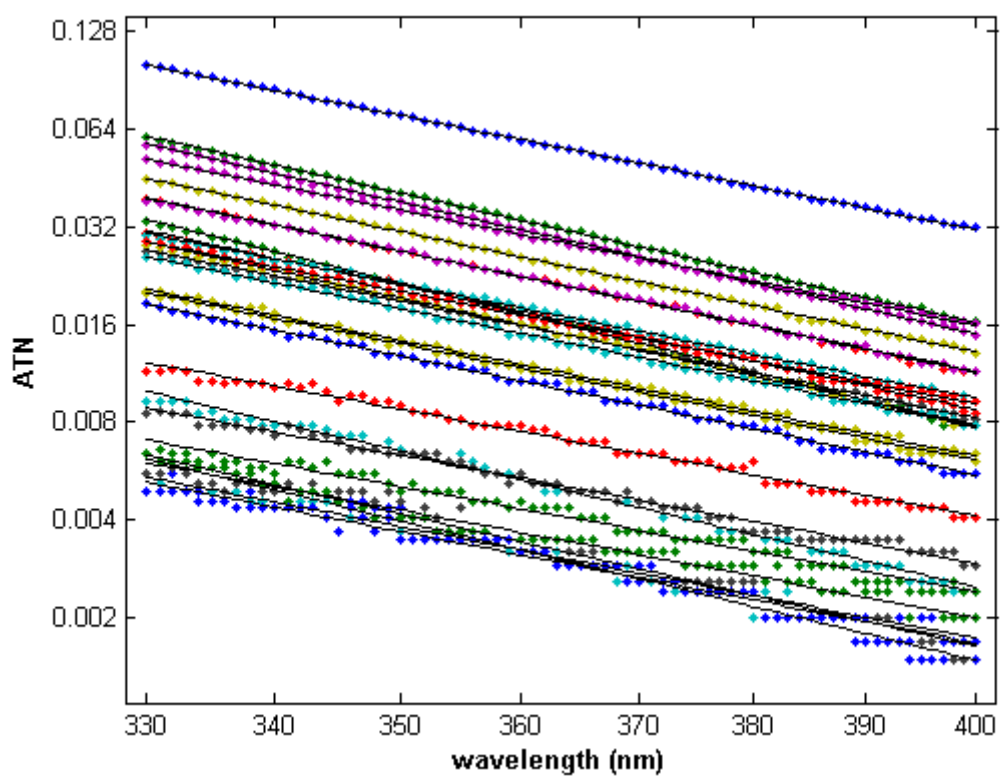


Figure S5. Wavelength dependent absorption spectra with the linear Ångström absorption coefficient (AAE) fitting for 13 TSP and PM_{2.5} samples extracted.

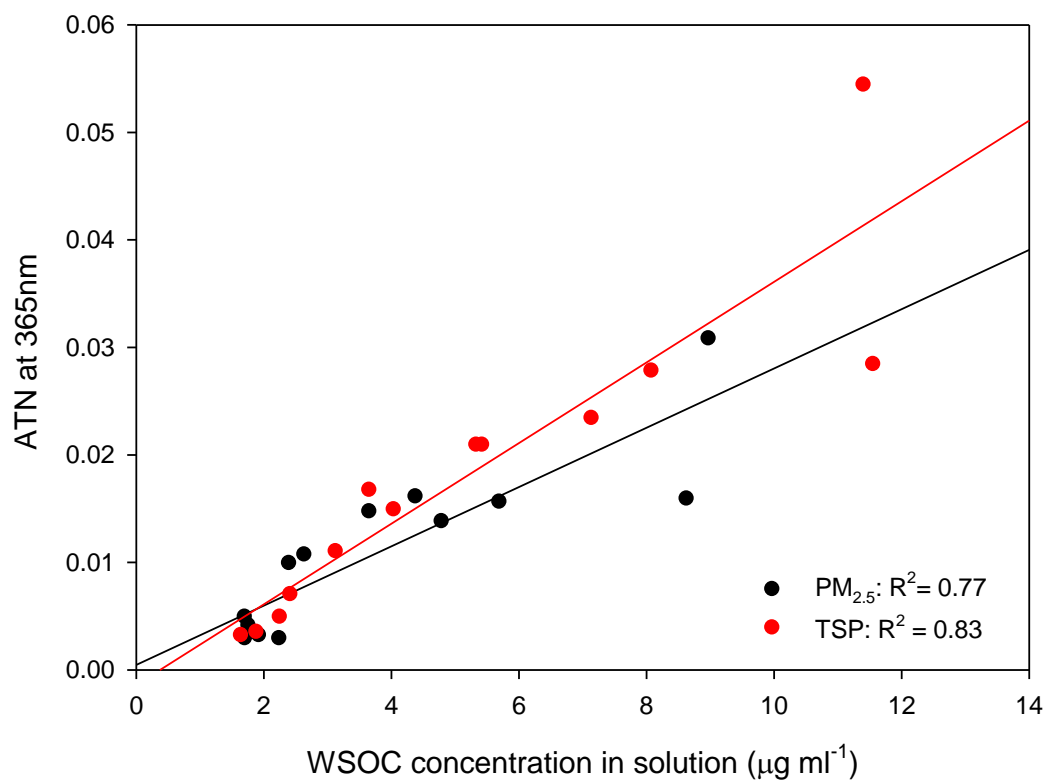


Figure S6. Relationship of the light attenuation coefficient (ATN) at 365 nm of the solution and the concentration of WSOC in the solution for 13 $\text{PM}_{2.5}$ and TSP extracts.

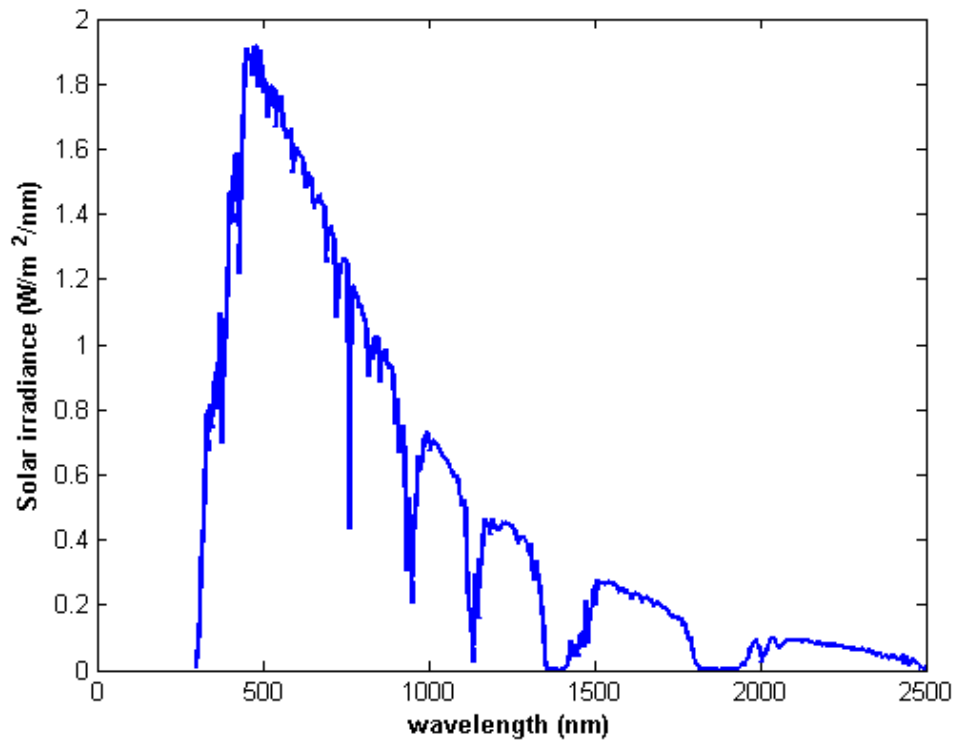


Figure S7. Plot showing the AM1GH model for solar irradiance, used for calculations of the relative radiative forcing model in Equations S1-2 (Levinson et al., 2010).

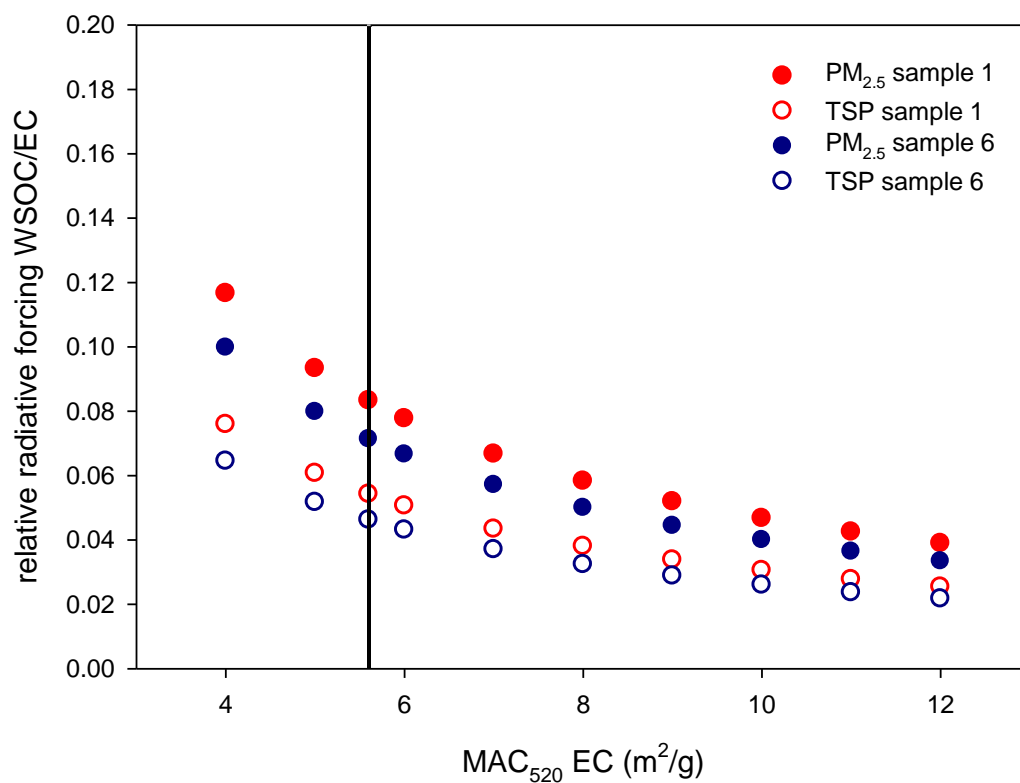


Figure S8. Dependency of the relative radiative forcing WSOC/EC, calculated using Equation (S3), on the value of $MAC_{520,EC}$. Two samples are depicted: sample 6 from the Beijing pollution plume and sample 10 from the Yellow Sea back trajectory cluster, for two size fractions (PM_{2.5} and TSP). The vertical line emphasize $MAC_{520,EC} = 5.6 \text{ m}^2/\text{g}$ (Chung et al., 2012) used in this paper.

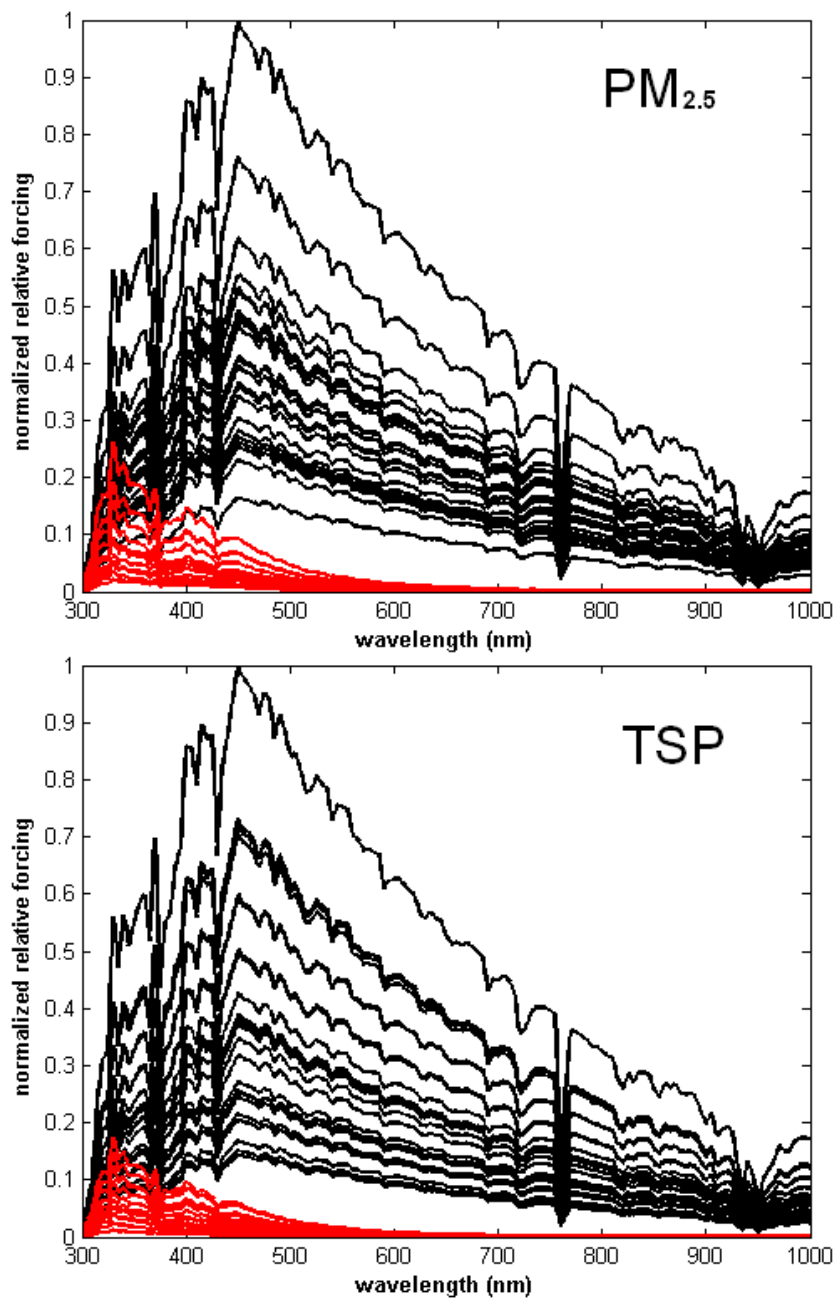


Figure S9. Normalized wavelength-dependence of the absorptive radiative forcing of water-soluble brown carbon (WSOC, red) relative to black carbon (BC, black) for observation of their light absorption in samples of the outflow originating in N China and intercepted during GoPoEx computed using the model outlined in SI Text.

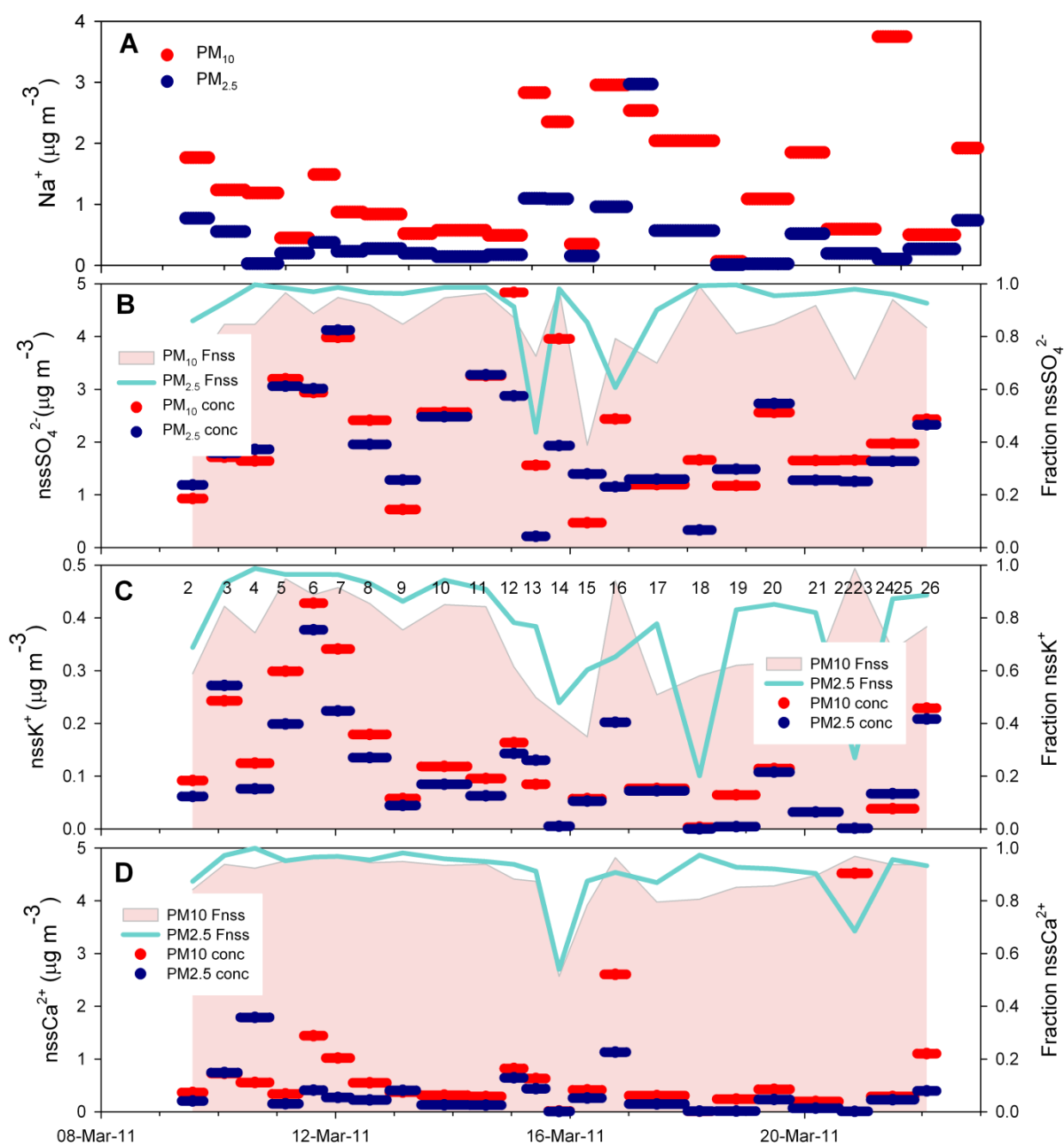


Figure S10. Concentrations of inorganic ions during GoPoEx campaign. Concentration of sodium (panel A). Concentrations of estimated non-sea salt sulfate, potassium and calcium and their relative fraction (as area plot for TSP and line plot for $\text{PM}_{2.5}$) of total measured concentration (panels B-D).